ELSEVIER

Journal of Nuclear Materials 266–269 (1999) 272–279

journal of nuclear materials

Limiter heat load and consequences on impurity source and transport

D. Guilhem [a,*], J. Hogan [b], T. Aniel [a], S. Boddeker [a], C. Grisolia [a], T. Hoang [a], G. Martin [a], B. Meslin [a], R. Mitteau [a], R. Reichle [a], J.C. Vallet [a]

[a] *CEN Cadarache, DRFC/SPPF, Association EURATOM-CEA, 13108 St Paul lez Durance, France*
[b] *Fusion Energy Division, ORNL, Oak Ridge, TN 37830, USA*

Abstract

Power deposition and consequences during short pulse operation $t < 2$ s, on non-actively cooled limiter (low field side) and large actively cooled inner-wall limiter (high field side) of Tore-Supra as well as long pulse operation $t > 20$ s (plasma limited by the inner wall) are reported. Infrared surface temperature measurements, thermocouples and Langmuir probes are used to diagnose the inner wall front face. They are presented for the first time and are complemented by measurements of a reciprocating Langmuir probe located at the top of the machine. A diagram of injected energy versus power shows how difficult it is to run high power long pulses in steady state conditions, which is one of the main goals for the next step fusion machine. An uncontrolled density rise is observed during long pulse operation ($P_{\mathrm{LHCD}} < 2.5$ MW, time duration > 20 s). It is believed that it is due *to recessed elements heated by plasma or due to fast particle losses due to the ripple*. The CIEL project will implement in Tore-Supra a set of actively cooled plasma facing components so that the performance of long pulse, high power shots should be improved.

Keywords: Graphite wall; Impurity release; Power handling; Thermal desorption; Water cooling

1. Introduction

The increase in auxiliary heating power in present day machines has led to the use of a large wetted area to reduce the heat flux, by tilting the field lines with respect to the normal of the surface. The particle and heat load on nearly tangent surfaces are still difficult to model. For toroidal limiters having a large poloidal extension with almost grazing angle of incidence, the usual power deposition equation must be modified to include a large local perpendicular heat flux [1]. Here we analyse a sequence of shots to understand the consequences of additional power (up to 11 MW) or long pulse operation (up to 120 s) and their effects on the main plasma parameters. Two configurations have been used: plasma leaning in one case on the large inner-wall (weakly inclined field lines) and the other case on the outboard limiter (field lines perpendicular at the leading edge). The inner wall has a faceted geometry with flat tiles on flat segments which have a general poloidal ($r \sim 0.82$ m) and toroidal ($R = 2.376$ m) radius of curvature. The main differences between these two plasma facing elements are (1) the large active area (12 m^2) and (2) the active cooling of the inner-wall, compared to the small (0.3 m^2) uncooled outboard limiter. The latter is a 'conventional' roof type pump limiter with two leading edges at the throat entrances on the ion and electron sides. These leading edges are close (0.015 m) to the last closed flux surface (LCFS), since the distance has been optimised for particle pumping, leading to large power heat flux densities >10 MW/m^2. The inner first wall is used for powerful and long duration discharges up to 2 min, despite being partly damaged (broken tiles due to pre-existing cracks // to the surface) by more than 10 years of operation [2]. A 60° sector of it was replaced by a new design using CFC cladding which proved to have

* Corresponding author. Tel.: +33 4 42 25 42 04; fax: +33 4 42 25 62 33; e-mail: guilhem@drfc.cad.cea.fr

0022-3115/99/$ – see front matter
PII: S0022-3115(98)00578-9

much improved bonding to the cooling structure compared to the previous using fine grain graphite. The radiation heated recessed plasma facing components seem to be the main limitation during long pulse operation. An uncontrolled electron density increase is observed after one minute operation ($I_p = 1$ MA, $\langle n_e \rangle = 2 \times 10^{19}$ m^{-3}, $P_{LHCD} = 2$ MW). This is neither correlated with the main gas injection nor with the main inner first wall surface temperature which is steady state. One observes however an oxygen contamination of the plasma presumed to be due to desorption of water from remote uncooled elements present in the machine, like ports, flanges [3] or ripple loss protections.

A large variety of plasma parameters have been analysed, $1 < P_{tot} < 11$ MW, $2 < Z_{eff} < 5$, 1 MW $< P_{rad} < 5$ MW, 1.5×10^{19} m^{-3} $< \langle n_e \rangle < 3.5 \times 10^{19}$ m^{-3}, 10 s $<$ duration < 120 s.

In the first part of the paper we study during short pulse operation (2 s during the heating phase) the different responses of the main plasma parameters in two different cases, one when the plasma is limited on the low field side by the outboard uncooled limiter and the other case when the plasma is limited on the high field side by the cooled inner wall. The second part is devoted to long pulse operation and the third part is a discussion of the experimental results. Finally we present briefly the CIEL project which is aimed at solving the difficulties we are facing so far during long pulse, high performance plasmas.

2. Experiment

Tore-Supra has a major radius of 2.4 m, a minor radius of 0.78 m and an almost circular plasma cross-section. The maximum power capability of the additional power is currently 6 MW for lower hybrid current drive (LHCD) and 10 MW for the ion cyclotron resonance heating (ICRH). So far the maximum power coupled to the plasma Fig. 1, is 11 MW total ($P_{ICRH} = 6.51$ MW, $P_{LHCD} = 4.66$ MW) during very short pulses of <2 s and 1.9 MW LHCD during long pulse operation of 117 s yielding 210 MJ of injected energy (1.8 MW on average during the whole discharge). Tore-Supra is equipped with a large number of core plasma and edge diagnostics: infrared thermography, reciprocating Langmuir probes and fixed Langmuir probes on the face of the inner wall.

3. Power scan during short pulse operation

An analysis of the Z_{eff} and radiated power is done to compare two situations, one where the plasma is leaning on the outboard limiter and the other one on the inner wall. In the latter case, Z_{eff} is slowly rising to 2.4 when

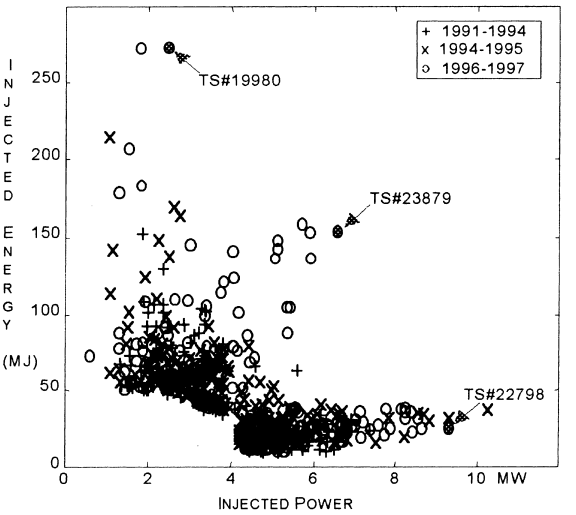

Fig. 1. Energy injected as a function of injected power. Less and less energy can be coupled to the plasma as the power is increased.

the additional power is increased to 9 MW for D_2 plasmas with $\langle n_e \rangle = 2.5 \times 10^{19}$ m^{-3} (consistent with the radiative scaling law [4]). The radiated power ranges 1–5 MW when up to 9 MW of auxiliary heating is used. On the other hand, when the plasma is leaning on the small uncooled outboard limiter, Z_{eff} and radiated power increase rapidly (more than linear) when the auxiliary power is increased, Fig. 2. This behaviour is not acceptable for long pulse operation since it leads inevitably to a core plasma contamination and eventually to plasma disruption. When the plasma is leaning on the inner wall the average electron density and radiated

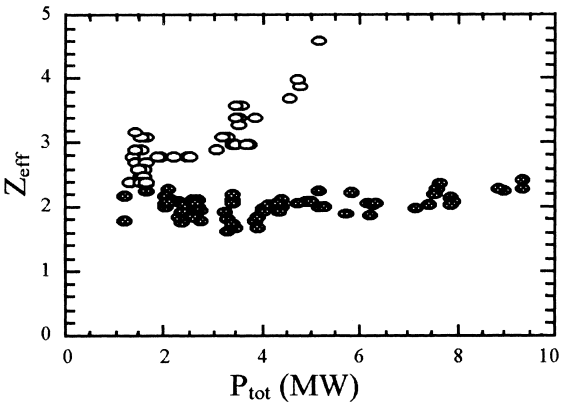

Fig. 2. Z_{eff} variation when ICRH power (D_2 plasmas) is increased in two different configurations: open circles when the plasma is limited by the uncooled outboard limiter; filled circles when the plasma is limited by the cooled inboard limiter.

power increase (compared to the preceding ohmic phase) with the total power. In this latter case, during long pulse operation, Z_{eff} stays low and constant, except at the very end, where we observe an electron density increase. Fig. 3 shows results from fixed Langmuir probes, located poloidally on the front face of the new CFC inner wall sector (located +10°, −15°, −25° and −45° from the equatorial plane). The effect of large additional power is to increase locally the recycling of particles, as indicated by a large increase of the density profile, while we observe a small modification on the temperature profile which is slightly increasing but stays below 15 eV. The reciprocating Langmuir probe located at the top of the machine indicate the same trend. This later shows large electron temperature and density e-folding lengths (~0.05 m) as indicated in Fig. 4. This behaviour is similar to what is observed on TFTR [5], a similar machine which has also a large graphite surface in contact with the plasma.

A diffusive 3D Monte-Carlo code THOR has already been used [1] to describe the diffusion of heat and hydrogenic particles across the last closed flux surface to the limiter located in SOL. A 3D field line tracing code taking into account the refined geometry is also used to understand such a power deposition pattern [6]. BBQ-code calculates impurity production and tracks impurity particle transport in the scrape-off layer, and as it penetrates, via radial diffusion, to flux surfaces 1 cm inside the LCFS [7,8]. It calculates the expected power dependence of impurity emission from a 'normal' inner wall due to physical sputtering. By 'normal' is meant the inner wall without defects or leading edges. Two sequences in which the power is steadily increased have been chosen: the first varying ICRF power from 2 to 6.5 MW, the second increasing LHCD power from 2 to 5 MW.

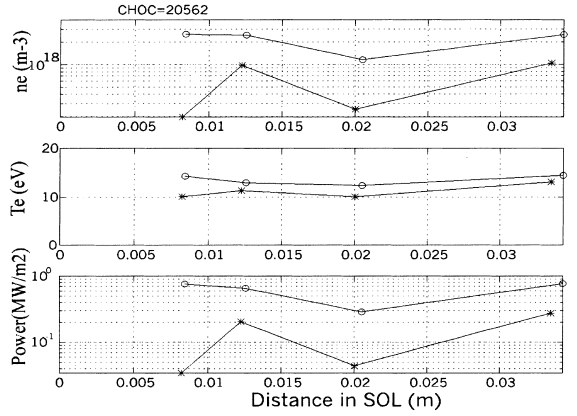

Fig. 3. Fixed Langmuir probes (located on the high field side at 10°, 15°, 30° and 45° from equatorial plane) profiles during the ohmic phase (stars) and when 6.5 MW of ICRH is injected in the plasma. Note the board profiles extending at least to the farthest probe located 7 cm in the scrape-off (45°).

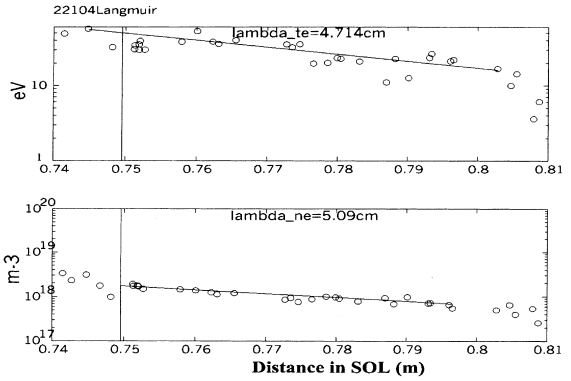

Fig. 4. Reciprocating Langmuir probe data (#22104). Note the broad electronic density and temperature profiles during long pulse operation ($P_{\text{LHCD}} = 2$ MW, $\langle n_e \rangle = 2.5 \times 10^{19}$ m^{-3}, $I_p = 1.2$ MA, time = 14 s).

In the code the detailed geometry has been used (to the level of individual tiles). The plasma configuration shows a slight non-circularity (increasing ellipticity with power) and this has been accounted for. The energy and particle flux dependence for the physical sputtering rates which are used have been taken from the formulae of Roth et al. [9], but increased in magnitude to fit the values measured by Mech et al. [10]. The scrape-off layer parameters have been taken from mobile probe measurements. Local flux amplification at the inner wall is assumed to increase from 1.5 to 3.0 as power increases. This is the level suggested from coupled B2–DEGAS calculations of the similar inner bumper limiter geometry in TFTR by Stotler et al. [11]. For some values in which mobile probe values are missing the scrape-off layer density and temperature have been interpolated between the higher and lower points in the power scaling sequence. Fig. 5 shows the radial profiles in the scrape-off layer for the carbon density from neutral carbon (C^0) through C^{3+} for the five cases in the ICRH power sequence.

For each sequence (ICRF, LHCD) the impurity generation due to physical sputtering of carbon by incident D^+ ions increases by up to 40% when the net (after radiation) incident power increases by greater than twofold, a trend which agrees with the observations of slowly rising core Z_{eff}. In all cases 60–65% of the generated impurities are re-deposited, and 35–40% penetrate deeper than 1 cm in the core plasma, where the BBQ calculation ceases to follow them. A notable trend as power increases is the increased density of the higher charge states (C^{3+}). These densities increase linearly with power, even though the neutral carbon density is roughly constant. This is due to the small increasing T_e

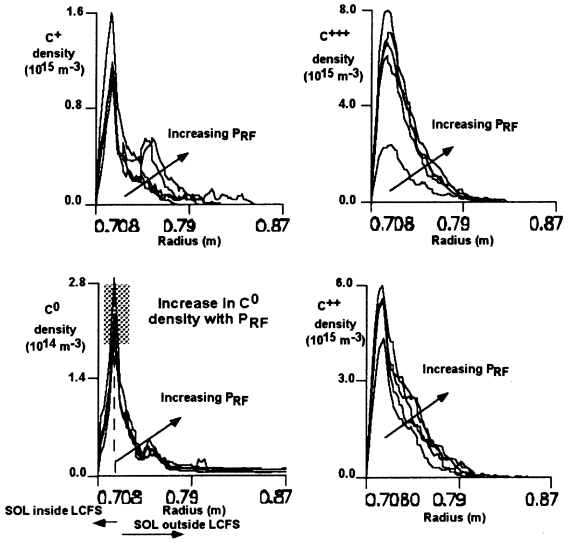

Fig. 5. Calculated radial profiles in the scrape-off layer for the carbon density from neutral carbon (C^0) through C^{3+} for the 5 cases in the ICRH power sequence ranging from 2 to 6.5 MW.

in the scrape-off layer as the power increases, which leads to a shorter lifetime for neutral carbon, and a higher scrape-off layer confinement time for the high charge states before the impurity ion either strikes the wall or enters the core plasma inside the LCFS. The central Z_{eff} is determined, subsequently, both by this impurity influx and by the core impurity confinement time. This, in turn, is determined by radial impurity transport: anomalous diffusivity, pinch (convection) terms, and sawtooth behavior. Thus, as long as confinement conditions (I_p, q_ψ, B_T) are kept fixed and we can expect ${t_p}^Z$ to be roughly constant, the scaling of central Z_{eff} with applied power should be proportional to product of the calculated impurity influx and the screening efficiency. Since the screening efficiency is 35–40% for all these cases, central Z_{eff} should scale directly as the impurity influx.

In contrast with the situation for the inner wall, where BBQ calculations indicate that more than 60% of the sputtered impurities are redeposited back to the inner wall, measurements and modelling of the outboard limiter geometry [12,13] show that the situation is reversed in that case: typically 60% of the sputtered impurities reach the core plasma, and 20% are redeposited on the limiter. Thus the screening efficiency is greater for the inner wall and we can expect roughly a 1.5–2 times larger increase in Z_{eff} for the same incident power flux, assuming 'quiescent' conditions. However, since the power handling capacity of the inner wall is higher than that of the outboard limiter 'non-quiescent' conditions, such super-brilliance' events, can occur and the Z_{eff} increase can be even larger.

4. Long pulse operation

Fig. 1 presents the Tore-Supra achievements in terms of energy as a function of power injected in the torus. One can observe that less and less energy can be handled when the injected power is increased. The pulse length limitation has been attributed in the past to the damaged inner wall tiles. The first generation of the inner wall was built in 1986, and this early realisation was subject to a certain number of difficulties associated with the quality of the brazed joint. Of the 8600 brazed tiles ~2% exhibited flaws, and the quality of the brazed joint was identified as the main difficulty in the industrial process. The number of identified damaged tiles has grown with time from 2% in 1988 up to 7% in 1994, probably because of the degradation of pre-existing defects. Since then, a 60° section of the wall has been replaced by a new technology, where CFC is attached by metal casting and electron beam welding on the cooled support structure. Non-destructive tests have been extensively used and only zero defect elements have been assembled. This sector is radially ahead of the old generation and did not suffer any damage so far. After realignment, a residual 'mechanical circle' shift of 1.8 mm of the inner wall and the "magnetic circle" of the toroidal coils in the equatorial plane, exist. Another difficulty we are facing, is the ability to couple a high level of both ICRH and LHCD power. We know that the antennas are interacting by shadowing effects and through plasma modification (mainly in the SOL) they induce. Strong toroidal asymmetries in power deposition are observed [14,15] during LHCD experiments. The experimental results indicate that fast electrons (estimated to be up to 2 keV) generated by the *rf* fields in the SOL in front of the antennas are responsible for the localised heat loads. They increase with both the edge density and the power level (electric field). The fraction of the injected power stays below 2% of the total injected power but the localised heat loads can be as high as tens of MW/m^2 (perpendicular to field lines). Nevertheless the global deposition heat flux on the inner wall is proportional to the total injected power which is consistent with modified one dimensional model [1] of the heat flux transmission through the sheath i.e. $Q \sim \gamma\ n_e\ T^{3/2} \sin(\theta + \theta_{\min})$. It is observed that T_e (LCFS) $\sim$ constant (<15 eV), n_e (LCFS) $\sim P_{\text{tot}}$ with small profile modification and so the inner wall heat flux is scaling as P_{tot} (when n_e is not large enough so that the plasma does not detach). Ion-neutral and charge-exchange collisions as well as ionisation within the SOL and the sheath have to play a major role here where probably neutral pressure is high.

A fixed infrared (3–5 μm) endoscope located on the low field side, measures the surface temperature map of the new CFC 60° inner wall panel. Fixed Langmuir probes are located on this sector. The system is cali-

brated from the ambient temperature of the cooled in-vessel components (usually 150–180°C) up to 2500°C. The calibration consists of an absolute calibration of the camera against a blackbody up to 2500°C and of an in situ calibration of the global transmission (0.6) of the infrared endoscope. This observed inner wall panel is also equipped with a set of seven thermocouples separated poloidally. They measure the temperature of the compliance layer between the CFC tile and the stainless steal heat sink. Finite element calculations allow to correlate their signals to the site (140 mm × 20 mm) averaged surface temperature, Fig. 6.

Apart from the peaking created by the ripple (<3 mm) the toroidal surface temperature profile is rather homogeneous. This is confirmed by the calorimetric measurements. They show a distribution of the removed power coherent with the relative positions of the panels (6 × 60° toroidally): +22% for the most advanced panel, −16% for the most recessed panel and + −5% to 10% for the rest. The surface temperature profile in the poloidal direction shows a strong peak at the equatorial plane, added to a rather broad background profile (temperature between shots = 150°C). This broad profile accounts for the majority of the power deposition. Infrared and thermocouple measurements (at the compliance layer) are coherent. The localised peak ($\lambda_q < 3$ mm) leads to a peak power density of 0.6 MW/m^2 deposition (which could be at least doubled without damage for the wall). It may be explained by a direct deposition of ions from the very edge of the plasma inside the LCFS, due to their finite Larmor radius (∼0.3 mm for 100 eV protons and ∼1 mm for 1 keV protons). This effect is strongest at the contact point of the plasma with the wall. The broadness of the rest of the surface temperature profile could be attributed to a large local fraction of neutrals (no measurements there) and radiated power since the ion conduction is low (as measured by the fixed Langmuir probes located on the wall face).

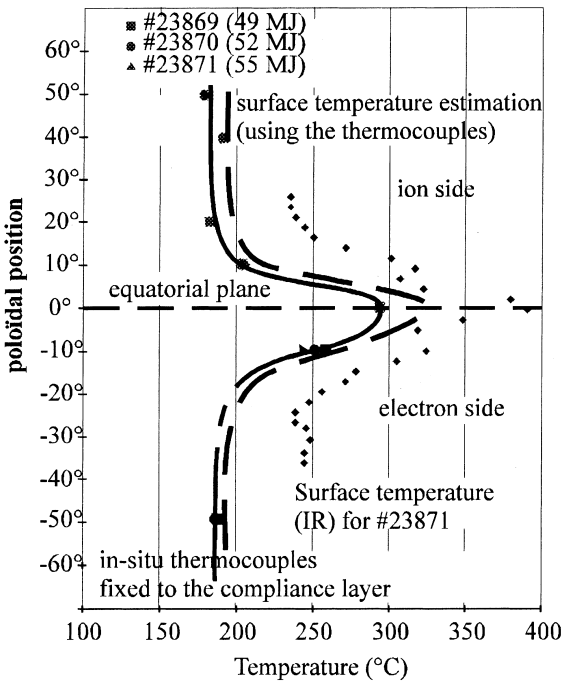

Fig. 6. Infared surface temperature and thermocouples profiles of a 60° section of the inner wall. Note the localised peak heat flux and the toroidally modulated deposition profile.

Two methods are used for the power balance analysis [16]. The first method uses the global measurements of the input power P_{in} and the local measurements (a) of the power flux to the inner wall, (b) the local measurements of the radiated power in 3 locations and (c) the charge collected by a detector of fast particles trapped in the magnetic field ripple (arriving in the upper vertical ports). Theses measurements are used to estimate the associated global power losses P_{dep}, P_{rad} and P_{rip}. This latter is assumed to be at least 20% of the ICRH power in these discharges [17] and is assumed to affect the vertical bolometers via charge exchange effects [18]. Since the ripple losses occur without contributing to the heating, the total power P_{tot} is calculated as $P_{tot} = P_{in} - P_{rip}$. The power balance is then achieved according to: $P_{tot} = P_{rad} + P_{dep}$. The second method is to compare the integral of the former quantities to global time-integrated calorimetric data. As a general example of long pulse operation, we have analysed (to within ±20%) the steady phase (after 6 s) for shot #23781 where $P_{ICRH} = 3.84$ MW, $P_{LHCD} = 2.00$ MW, $P_{Ohmic} = 0.28$ MW corresponding to 6.12 MW total injected power. Total extracted power breaks into $P_{rip} = 0.85$ MW, $P_{rad} = 1.87$ MW and finally $P_{dep} = 3.65$ MW. The comparison with the calorimetry suggests that the estimate of P_{dep} via the power balance is rather an upper limit and the other two estimates are close to the lower limit of their error bar.

During low power ($P < 2.5$ MW), low density ($\langle n_e \rangle = 10^{19}$ m^{-3}), long pulse operation ($t > 40$ s), an increase in volume averaged electron density is observed after 60 s, Fig. 7. This onset time before an uncontrolled electron density increase occurs, depends on the absolute radiated power: more radiated power (or $\langle n_e \rangle$ core density) corresponds to shorter onset times. The carbon C_{VI} line decreases as the density increases, contrarily to the oxygen O_{VIII} line which starts to increase rapidly. One possible interpretation of this time behaviour of the electron density increase is that it is due to photon induced desorption of water from the recessed elements not in direct contact with the plasma, principally uncooled port sides, flanges [3]. Another explanation is the large power heat load of non actively cooled ripple loss protections. As the density increases, the radiated power increases leading to the release of oxygen. This is an unstable situation, which could lead eventually to

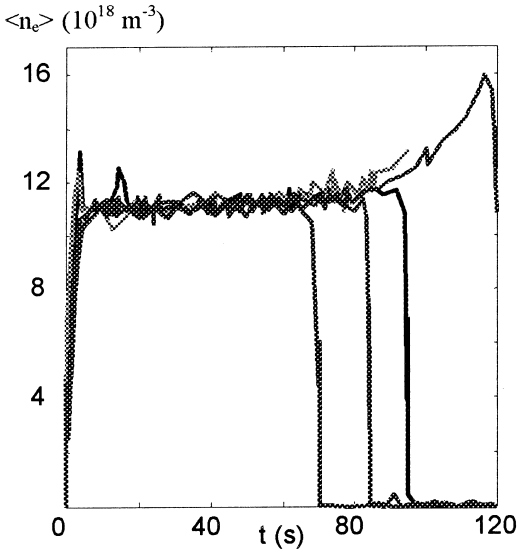

Fig. 7. Time evolution of the volume averaged electron plasma in a serie of long pulse operation.

disruption. On the one hand, the main actively cooled inner-wall limiter reaches steady state after a few tens of seconds. On the other hand, the recessed elements are heated continuously by plasma radiation (5 kW/m^2 during 100 s on a thick stainless steel flange leads to a temperature increase of 17°C, large enough compared to its 50°C normal temperature to lead to a large desorption) and are possibly responsible for the oxygen contamination (water desorption). Another explanation could be associated with the substantial ripple losses. With 20% of the injected power being concentrated on areas of typically 18 coils × 10 cm × 10 cm maximum, with some peaking of a factor 2 in the middle (corresponding to almost 10 MW/m^2) one would expect a large temperature rise and so a large desorption of any gases contained in the CFC ripple loss protections. To obtain a really steady state regime as is needed for ITER, one has to cool all the vessel elements, i.e. elements in direct contact with the plasma (limiters) and elements not in direct contact with the plasma but in direct view of it (protection limiter and wall, ripple loss protection elements, ports, flanges, etc.). This is why we are preparing the CIEL project for Tore-Supra (implemented during year 2000), which will provide an upgrading of all the inner vessel components in order to improve the heat and particle exhaust capabilities.

5. Discussion

As indicated by the fixed and reciprocating Langmuir probes, the infrared surface temperature and the thermocouple measurements, the power deposition shows a rather complex pattern. The infrared surface temperature measurements present a toroidal modulation and a peaked poloidal profile on top of a broad one. The maximum surface temperature and hence power deposition are maximum at the toroidal locations where the magnetic field ripple is maximum, i.e. between coils. This is not compatible with the simple picture of the model taking into account the parallel heat flux without a minimum angle of incidence. This peak could be explained by direct deposition of ions from inside the LCFS at a distance less than one Larmor radius. We can also notice a modulation as a function of time, of the surface temperature at locations where temperature is maximum, correlated with the plasma current modulation ($\Delta I_p/I_p = 10\%$). This modulation is not observed at locations where the surface temperature is minimum (under coils where the ripple is minimum), locations where fixed Langmuir probes are located. Indeed these probes do not show any electron temperature or density modulation as a function of time. The poloidal temperature profiles present a peaked profile on top of a broad profile which is responsible for the majority of the power load. The toroidal distribution of the extracted energy is measured by water calorimetry of the cooling loop on six sections of 60° equally spaced toroidally (no poloidal resolution since it is integrated on the 150° poloidal extension of each section). These measurements indicate a toroidal distribution variation, from −16% for the most recessed section, to +22% for the most advanced section, compared to the averaged value. The thermocouples poloidal profile is consistent with the infrared surface temperature profile. This gives confidence in the measurements which indicate that the broad profile is responsible for the main part of the power deposition on the inner wall.

Reciprocating Langmuir probe located at the top of the machine away from the inner wall, indicates as well broad electron temperature and density profiles (e-folding length ∼ 0.05 m). The electron temperatures and densities at the LCFS are measured to range 17–28 eV and 5×10^{18}–7×10^{18} m^{-3} when the ICRH is increased from 2 to 6.5 MW. They range 24–37 eV and 1.5×10^{18}–4×10^{18} m^{-3} when LHCD power is increased from 2 to 6 MW.

Fixed Langmuir probe profiles indicate at the inner wall face, that the electron temperature is slowly rising (from 10 to 15 eV) when the additional power is increased from ohmic to 6.5 MW ICRH, contrarily to the density profile which is proportional to the injected power. The poloidal electron density profile is hollow in the ohmic phase and almost flat when the additional power reaches 6.5 MW. The modelling indicates that the inner wall configuration is much better at screening the produced impurities (carbon assumed to be the dominant specie), with 60% direct redeposition than the outboard limiter configuration where only 20% is

re-deposited. This can be probably explained by the fact that the inner wall is localised on the low field side where, due to the Shafranov shift, electron temperature is lower (<15 eV) and due to the lower density and power load, the impurity source is much lower.

6. CIEL project

The CIEL project [19] will provide an upgrading of all the inner vessel components in order to improve the heat and particle exhaust capabilities: a toroidal pump limiter, a pumping system, vacuum vessel protection, guard limiters Fig. 8 and later, protections for the rf antennas. The toroidal pump limiter is an annular disk ($R_i = 2.2$ m, $R_o = 2.715$ m, 0.51 m long in radial direction). It covers 7.5 m^2 of the bottom area of the machine (2.5 m^2 will be wetted by the plasma $r = 0.72$ m, $R = 2.4$ m, $\lambda_q = 0.015$ m). This limiter has been designed to remove permanently a total convective power of 15 MW, leading to a peak heat flux of 10 MW/m^2. Twelve of the 18 port locations are equipped with pumping throats equipped with V shaped target plates which are connected two by two to five cryo-mechanical pumps capable to pump all gases (D_2, He, Ne, Ar...). A total particle exhaust efficiency of ~10% is expected.

An actively cooled inner wall protection will cover all the rest of the inside vessel. Lots of efforts have been made to decrease to ~2% the overall transparency of this protection wall so that the vacuum vessel is entirely protected against conducted (suprathermal electrons due to LHCD, fast ions and electrons which are trapped in the magnetic ripple) and radiated power (up to 1 MW/m^2), allowing plasma operation for several thousands seconds per day.

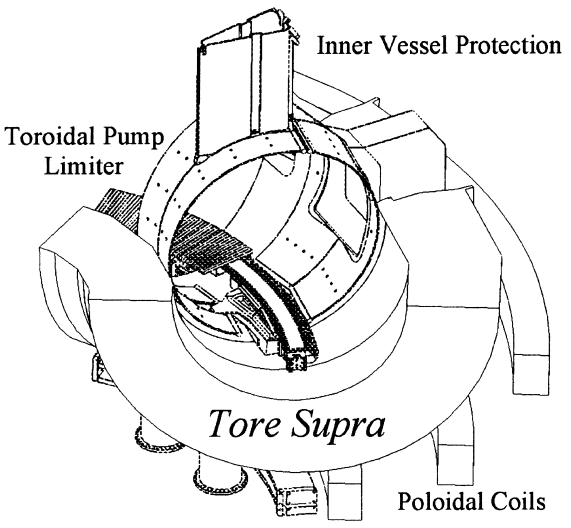

Fig. 8. General view of the in-vessel elements which all are actively cooled (transparency <2%).

Six actively cooled poloidal bumpers are placed on the high field side, equally spaced, for start-up and disruption protection. They are placed 4–5 λ_q in the SOL and will receive only 0.5 MW/m^2 (400°C steady-state) corresponding to a scenario where 15 MW are conducted to the toroidal limiter and where 10 MW is radiated. They can sustain also the most severe disruptions (500 kJ, 60 MeV).

7. Conclusions

High power (11 MW–2 s–33 MJ), long pulse (117 s–210 MJ–1.9 MW or 272 MJ–113 s–$P_{LHCD} = 2.5$ MW) and moderate power with relatively long (7 MW–20 s–150 MJ) pulse operation have been achieved in Tore-Supra. The main limiter is a large (12 m^2) actively cooled inner wall, capable to extract up to 10 MW in a steady state regime (time constant = 20 s). It has been shown that Z_{eff} is rising slowly as the injected power was increased when the plasma was limited by the actively cooled inner wall. We do not observe any Z_{eff} increase during the first tens of seconds of long pulse discharges. After this time, a plasma electron density increase is observed, principally due to oxygen contamination possibly due to water desorption. *The main limitation comes from the recessed elements not actively cooled (ripple loss protections, protection limiter not in contact with the plasma, ports, flanges, etc.) which heat up during plasma operation*. This temperature increase of remote vessel elements leads to an oxygen contamination of the core plasma, situation which can eventually lead to a plasma disruption.

Taking into account these difficulties, we have designed for the CIEL project new plasma facing components. All the elements installed in the vacuum vessel facing the plasma will be actively cooled so that successful long pulse, high power operation can be expected.

Acknowledgements

Thanks to H. Roche and J.Y. Pascal for their help in data collection and analysis.

References

[1] A. Seigneur, D. Guilhem, J. Hogan et al., Proceedings of the 20th Euro. Conf. Contr. Fusion and Plasma Phys., Lisbon, Portugal, vol. 2, European Physical Society, 1993, p. 603.
[2] Equipe TORE-SUPRA, Fusion Technol. 29 (1996) 417.

[3] Tore-Supra Team presented by C. Grisolia, these Proceedings.
[4] G. Mattews et al., J. Nucl. Mater. 241–243 (1997) 450–455.
[5] C.S. Pitcher, P.C. Stangeby, J. Nucl. Mater. 196–198 (1992) 241–247.
[6] R. Mitteau, A. Moal, J. Schlosser, D. Guilhem, these Proceedings.
[7] J. Hogan, C. Klepper et al., IAEA-CN-64/DP-15, 1996.
[8] J. Hogan et al., Integrated impurity model for actively cooled plasma-facing components, Plasma Phys. and Contr. Fusion Research, Proceedings of the 16th International Conference, Montreal, 1996, IAEA Vienna, 1997, to be published.
[9] J. Roth, C. Garcia-Rosales, Nucl. Fusion 36 (1996) 1647.
[10] B.V. Mech, A.A. Haasz, J.W. Davis, J. Nucl. Mater. 241 (1997) 1147.
[11] D. Stotler et al., IEEE Trans. Plasma Sci. (Oakland) 88 (1990).
[12] S. Tobin, J. Hogan, C. DeMichelis et al., Plasma Phys. Contr. Fusion 38 (1996) 251.
[13] S. Tobin, C. DeMichelis, J. Hogan. et al. Plasma Phys. Contr. Fusion, accepted for publication.
[14] J.H. Harris et al., J. Nucl. Mater. 241–243 (1997) 511–516.
[15] J. Mailloux et al., J. Nucl. Mater. 241–243 (1997) 745–749.
[16] R. Reichle, J.C. Vallet, M. Chantant, V. Basiuk, A. Grosman, D. Guilhem, Towards a global power balance in Tore-Supra, to be published at EPS-1998, Prague, private communication.
[17] V. Basiuk et al., Nucl. Fusion 35 (1995) 12.
[18] J.C. Vallet, C. Balorin, M. Jouve, M. Mattioli, A.L. Pecquet, D. Guilhem, The new bolometric diagnostic on Tore-Supra, EPS Berchtesgaden 97, P1.059.
[19] M. Lipa et al., Proceedings of the 17th IEEE/NPSS Symposium on Fusion Engineering, San Diego, California, vol. 1, Institute of Electrical and Electronics Engineers, Inc., Piscataway, 1998, p. 353.